NUMERICAL SIMULATION OF COASTAL INUNDATION OVER DISCONTINUOUS TOPOGRAPHY

Sung Bum Yoon and Ji Hoon Cho

Department of Civil and Environmental Engineering, Hanyang University, Kyunggi, Korea

Abstract: A new moving boundary technique for leap-frog finite difference numerical model is proposed for the reasonable simulation of coastal inundation over discontinuous topography. The new scheme improves the moving boundary technique developed by Imamura(1996). The present scheme is tested using the analytical solution of Thacker(1981) for the case of free oscillation with moving boundary in a parabolic bowl. Finally, a numerical simulation is conducted for the flooding over a tidal barrier constructed on a simple concave geometry. A general feature of inundation over a discontinuous topography is well described by the numerical model.

Key Words: moving boundary, leap-frog finite difference model, discontinuous topography

1. INTRODUCTION

The inundations occurred in the coastal area of Korea are caused either by the superposition of astronomical and meterological tides in the western coast, or by the tsunamis, in the eastern coast, generated in the subduction area located along the west coast of Hokkaido and Honshu, Japan.

During the period of Aug. 19~21 in 1997 an extraordinary high tide due to the combination of spring tide and the meteorological effect of typhoon, Winnie, occurred along the west coast of Korea. The sea level rise above the predicted ordinary water level was observed as 63cm at Inchon, 77cm at Anhung, 60cm at Boryung, 71cm at Kunsan and 32cm at Mokpo. This high tide had caused the flooding in many reclamated rice field. The property damage due to this high tide was estimated as 22 billion Korean wons.

The tsunami, generated by the earthquake (JMA scale 7.7) in the western sea area of Akita prefecture of Japan in 1983, killed 104 people and destroyed 5,000 houses in Japan. The tsunami propagated westward and attacked the east coast of Korea. Two people were missing and other two were wounded. The sea level rise at Imwon was recorded as 3.6~4m above the normal tide level and the maximum fall down was 5m below tide level.

For the prediction of inundation process in the coastal area, it is essential to calculate the water surface elevation using the hydrodynamic numerical models which can deal with moving boundary with reasonable accuracy.

Yoon et al. (1994) developed a leap-frog fi-

nite difference numerical model which employs the moving boundary scheme proposed by Iwasaki & Mano(1979). This model can solve the inundation problem over a slowly varying topography even for the case of no bottom friction. In their numerical model, a special care is taken for the continuation of advection effect across the moving boundary. This scheme has been adopted in the tsunami numerical model of Cornell research group for the simulation of inundation at Hilo harbor of Hawaii caused by 1960 Chilean Tsunami Event(Liu et al., 1995; Cho, 1995). The numerical model of Yoon et al. (1994) and Cornell research group can be successfully applied to the case of inundation over slowly varying topography. However, this model may give unrealistic solution for a discontinuous topography such as breakwater, tidal barrier and hydraulic structures with a steep slope.

On the other hand, Imamura(1996, actually much earlier than this) developed a moving boundary technique suitable for discontinuous depth region. This scheme is implemented in the tsunami numerical models of Tohoku research group. Since the advection effect is dropped for a few cells adjacent to the moving boundary, Tohoku numerical model is unstable if the bottom friction is absent.

In this study, the moving boundary scheme proposed by Imamura(1996) is first introduced, and is improved by continuing nonlinear effects across the moving boundary. The new scheme is tested for the cases of free oscillation in the parabolic bowl. The numerical solution is compared with the analytical solution derived by Thacker(1981). The present numerical model is then applied for the inundation of sea water over a conceptual topography with depth discontinuity.

2. GOVERNING EQUATIONS

Since the coastal inundation is generally induced by long waves such as tide, storm surges and tsunamis, the shallow water equations can be employed(Goto & Shuto, 1983):

$$\frac{\partial \eta}{\partial t}+\frac{\partial P}{\partial x}+\frac{\partial Q}{\partial y}=0 \tag{1}$$

$$\frac{\partial P}{\partial t}+\frac{\partial (P^2/D)}{\partial x}+\frac{\partial (PQ/D)}{\partial y}+gD\frac{\partial \eta}{\partial x}+\frac{gn^2}{D^{7/3}}P\sqrt{P^2+Q^2}=0 \tag{2}$$

$$\frac{\partial Q}{\partial t}+\frac{\partial (PQ/D)}{\partial x}+\frac{\partial (Q^2/D)}{\partial y}+gD\frac{\partial \eta}{\partial y}+\frac{gn^2}{D^{7/3}}Q\sqrt{P^2+Q^2}=0 \tag{3}$$

where η represents the free surface displacement measured upwards from still water level(m), P and Q are the depth-averaged volume fluxes(m^2/s), and h is the water depth(m) measured upwards from the bottom to still water level. n denotes the Manning's roughness coefficient($sec/m^{1/3}$), and D is the total water depth. Thus, the total water depth can be obtained using h and η as:

$$D=h+\eta \tag{4}$$

Fig. 1 presents the definition sketch of various depths and levels used in this study.

3. NUMERICAL SCHEME

The numerical model employed in the present study is basically the same as that developed by Imamura(1996) with some improvements on the nonliear terms near the wave front made by Yoon et al.(1994).

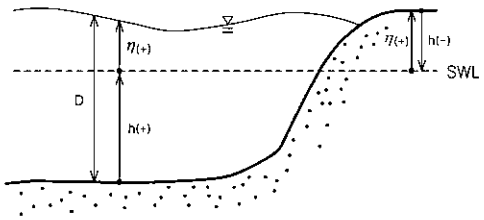

Fig. 1. Definition sketch of various water depths and levels.

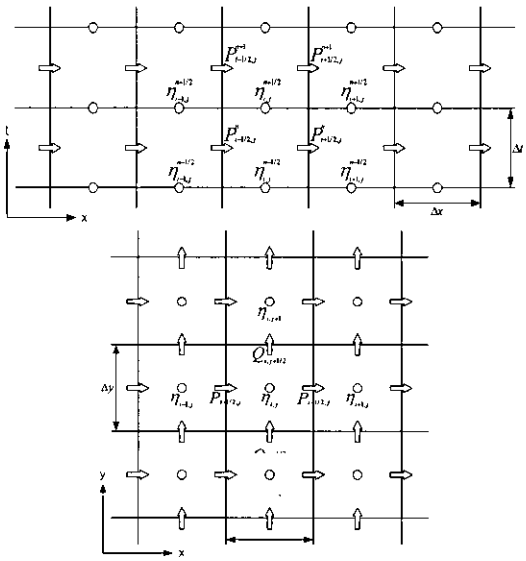

Fig. 2. Staggered mesh used in the leap-frog finite difference scheme.

The present model solves (1)~(3) on a staggered mesh using finite difference leap-frog scheme as shown in Fig. 2. The finite difference representations of (1)~(3) are given as:

$$\frac{\eta_{i,j}^{n+1/2}-\eta_{i,j}^{n-1/2}}{\Delta t}+\frac{P_{i+1/2,j}^{n}-P_{i-1/2,j}^{n}}{\Delta x}+\frac{Q_{i,j+1/2}^{n}-Q_{i,j-1/2}^{n}}{\Delta y}=0 \tag{5}$$

$$\frac{P_{i+1/2,j}^{n}-P_{i+1/2,j}^{n}}{\Delta t}+M_{PP}+M_{PQ}+gD_{i+1/2,j}^{n+1/2}\frac{\eta_{i+1,j}^{n+1/2}-\eta_{i,j}^{n+1/2}}{\Delta x}+F_P=0 \tag{6}$$

$$\frac{Q_{i,j+1/2}^{n}-Q_{i,j+1/2}^{n}}{\Delta t}+N_{PQ}+N_{QQ}+gD_{i,j+1/2}^{n+1/2}\frac{\eta_{i,j+1}^{n+1/2}-\eta_{i,j}^{n+1/2}}{\Delta y}+F_Q=0 \tag{7}$$

where the subscripts i and j denote the grid point number in x and y directions, respectively. n is the time step number. Δx and Δy represent the grid size in x and y directions, respectively, and Δt is the time increment.

M_{PP}, M_{PQ}, N_{PQ} and N_{QQ} in (6) and (7) represent the nonlinear advection terms which can be approximated by the following upwind technique as:

$$M_{PP}=\frac{1}{\Delta x}\left[(P^2/D)_{i+1/2,j}^{n}-(P^2/D)_{i-1/2,j}^{n}\right],\quad if\quad P_{i+1/2,j}^{n}>0 \tag{8}$$

$$M_{PP}=\frac{1}{\Delta x}\left[(P^2/D)_{i+3/2,j}^{n}-(P^2/D)_{i+1/2,j}^{n}\right],\quad if\quad P_{i+1/2,j}^{n}\le 0 \tag{9}$$

$$M_{PQ}=\frac{1}{\Delta y}\left[(PQ/D)_{i+1/2,j}^{n}-(PQ/D)_{i+1/2,j-1}^{n}\right],\quad if\quad Q_{i+1/2,j}^{n}>0 \tag{10}$$

$$M_{PQ}=\frac{1}{\Delta y}\left[(PQ/D)_{i+1/2,j+1}^{n}-(PQ/D)_{i+1/2,j}^{n}\right],\quad if\quad Q_{i+1/2,j}^{n}\le 0 \tag{11}$$

$$N_{PQ}=\frac{1}{\Delta x}\left[(PQ/D)_{i,j+1/2}^{n}-(PQ/D)_{i-1,j+1/2}^{n}\right],\quad if\quad P_{i,j+1/2}^{n}>0 \tag{12}$$

$$N_{PQ}=\frac{1}{\Delta x}\left[(PQ/D)_{i+1,j+1/2}^{n}-(PQ/D)_{i,j+1/2}^{n}\right],\quad if\quad P_{i,j+1/2}^{n}\le 0 \tag{13}$$

$$N_{QQ} = \frac{1}{\Delta y}\left[(Q^2/D)^n_{i,j+1/2} - (Q^2/D)^n_{i,j-1/2}\right], \quad if \quad Q^n_{i,j+1/2} > 0 \tag{14}$$

$$N_{QQ} = \frac{1}{\Delta y}\left[(Q^2/D)^n_{i,j+3/2} - (Q^2/D)^n_{i,j+1/2}\right], \quad if \quad Q^n_{i,j+1/2} \le 0 \tag{15}$$

where the variables (e.g., $Q^n_{i+1/2,j}$ and $P^n_{i,j+1/2}$ etc.) which are not assigned on a grid point are evaluated by the interpolation of variables at four surrounding grid points as:

$$Q^n_{i+1/2,j} = \frac{1}{4}(Q^n_{i,j+1/2} + Q^n_{i+1,j+1/2} + Q^n_{i,j-1/2} + Q^n_{i+1,j-1/2}) \tag{16}$$

$$P^n_{i,j+1/2} = \frac{1}{4}(P^n_{i+1/2,j+1} + P^n_{i+1/2,j} + P^n_{i-1/2,j+1} + P^n_{i-1/2,j}) \tag{17}$$

The bottom friction terms F_P and F_Q are solved by an implicit scheme to have stable solutions as:

$$F_P = \frac{gn^2}{2}\left[\frac{\sqrt{P^2+Q^2}}{D^{7/3}}\right]^n_{i+1/2,j}(P^{n+1}_{i+1/2,j} + P^n_{i+1/2,j}) \tag{18}$$

$$F_Q = \frac{gn^2}{2}\left[\frac{\sqrt{P^2+Q^2}}{D^{7/3}}\right]^n_{i,j+1/2}(Q^{n+1}_{i,j+1/2} + Q^n_{i,j+1/2}) \tag{19}$$

When the total water depth D approaches to zero at the wave front, the bottom friction increases infinitely and the run-up and run-down process become unrealistic. Thus, the total water depth D in the friction terms is limited to be greater than the predetermined depth, say, 0.01m. The total water depths D assigned on P and Q grid points in the equations of motion (5) and (6) are evaluated as:

$$D^{n+1/2}_{i,j} = h_{i,j} + \eta^{n+1/2}_{i,j} \tag{20}$$

$$D^{n+1/2}_{i+1,j} = h_{i+1,j} + \eta^{n+1/2}_{i+1,j} \tag{21}$$

$$D^{n+1/2}_{i,j+1} = h_{i,j+1} + \eta^{n+1/2}_{i,j+1} \tag{22}$$

$$D^{n+1/2}_{i+1/2,j} = \frac{1}{2}(D^{n+1/2}_{i+1,j} + D^{n+1/2}_{i,j}) \tag{23}$$

$$D^{n+1/2}_{i,j+1/2} = \frac{1}{2}(D^{n+1/2}_{i,j+1} + D^{n+1/2}_{i,j}) \tag{24}$$

The total water depth $D^n_{i,j}$ in nonlinear advection terms and friction terms can be found as:

$$D^n_{i,j} = h_{i,j} + \frac{1}{2}(\eta^{n+1/2}_{i,j} + \eta^n_{i,j}) \tag{25}$$

Thus, the total water depths at n th time step on the grid point for P and Q can be evaluated by the interpolation of the values on the surrounding grid points as in (23) and (24).

4. MOVING BOUNDARY TECHNIQUE

The water front, a boundary between water body and land, moves forward and backward as the water level fluctuates up and down at the coastline. The moving boundary technique developed by Imamura(1996) approximates first the real topography by a series of steps with a narrow width as shown in Fig. 3.

The water depth h is positive when the elevation of bottom is under the still water level, and is negative for opposite situation. If the total water depth D at the grid point is positive,

then the grid point is wet or submerged. On the other hand, if D is zero, the cell is dry or exposed. Thus, for the dry area, the free surface displacement η should be set as $-h$ to give a zero total depth for exposed area.

When a rundown of waves occurs, a thin film of water is left on the exposed bottom due to excessively high bottom friction after a main water body is removed. Since the location of boundary can not be clearly identified in this case, it is necessary to replace η by $-h$ for this area where the total water depth D is less than a predetermined minimum depth.

For simplicity, various situations involved in wet/dry problem are presented in Fig. 4 only for one dimensional inundation. The wet/dry boundary is located at the flux grid point of $i+1/2$. In the figure, the cases of (a1) and (c1) represent the exposed area, and the flux $P_{i+1/2}$ is set as zero. (b3) and (d3) show the normal wet

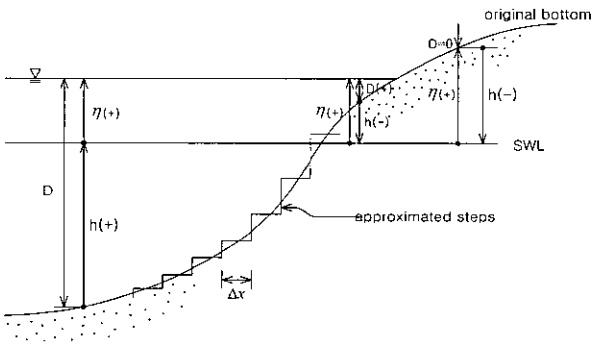

Fig. 3 Approximation of topography by steps and definition of various water depths

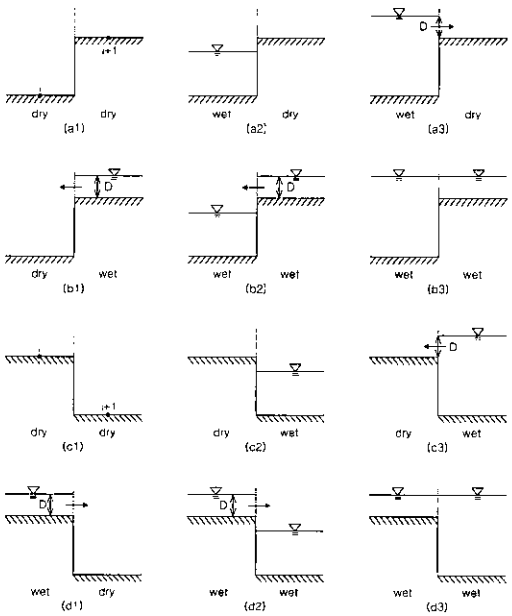

Fig. 4 Dry/wet situation at i+1/2 point and moving boundary (Imamura, 1996); (a) & (b), $-h_i < -h_{i+1}$; (c) & (d), $-h_i > -h_{i+1}$

area and the flux $P_{i+1/2}$ can be determined with no special care. (a2) and (c2) represent the situation where the wet/dry boundary is located between wet and dry cells. Since the water surface in the wet cell is lower than the bottom of dry cell, the boundary stays at grid point $i+1/2$ and the flux P is set to be zero. (a3), (b1), (c3) and (d1) represent the cases where the wet/dry boundary is located at $i+1/2$ point at the present time step, but the dry cell will be inundated. The flux P is calculated using the equation of motion with the total water depth D shown in the figure and the surface gradient $D/\Delta x$. The boundary moves to the next grid point. Finally, the cases of (b2) and (d2) do not involve the wet/dry boundary, but a special care is taken when the surface gradient in the equation of motion is evaluated. The water body in the lower cell does not affect the flow downward from the upper cell. In Yoon et al.(1994), the 6 cases of (a3), (b1), (b2), (c3), (d1), and (d2) are treated in a different way from the present one described above.

The moving boundary scheme discussed above becomes complicated when two dimensional inundation is involved. Moreover, the advective terms give further difficulties in developing algorithm to deal with the cells near the moving boundary, because the upwind scheme uses the information outside the computational domain depending on the flow direction at flux point near the boundary. Thus, the nonlinear advection terms are neglected for three grid points near the moving boundary (Imamura, 1996). However, the advective term increases all the way towards the moving boundary and reaches the maximum there. If the bottom friction is neglected, some disturbances due to discontinuities in water surface and fluxes are triggered between the cells where the advection terms are included and are excluded. The disturbances grow with time and the solution becomes unstable. This instability is more prominent during rundown process.

Yoon et al.(1994), Liu et al.(1995) and Cho(1995) improved the moving boundary scheme proposed by Iwasaki & Mano(1979) by making the advection effect be continuous near the boundary. In this study, the moving boundary scheme developed by Imamura(1996) is improved by borrowing the idea of Yoon et al.(1994).

5. NUMERICAL TEST OF RUN-UP MODEL

The observed or measured data for the verification of present inundation model are rare in the literature. In this study, the accuracy of run-up model is tested using the analytical solution of nonlinear shallow-water equations developed by Thacker(1981). The Thacker's solution is exact for the case of long wave oscillation in the parabolic bowl as shown in Fig. 5. Since the effect of bottom friction is neglected in the analytical solution, the original inundation model developed by Imamura(1996, actually this model was developed much earlier, but appears first in the literature in 1996) can not be employed due to instability problem in his model.

In Fig. 5, D_0 and L represent the maximum water depth and the distance from the center of bowl to the coastal line, respectively, when the water is at rest. R_0 is the distance from the center of bowl to the coastal line when the free surface displacement η at the center becomes maximum. If D_0, L, and R_0 are given, the still water depth h, angular frequency of oscillation ω, and nondimensional

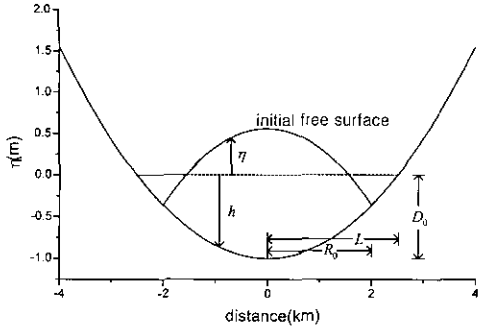

Fig. 5. Drfinition of variables for the free oscillation in a parabolic bowl

parameter A are determined for any point with distance r from the center as:

$$h = D_0\left[1-\frac{r^2}{L^2}\right] \tag{26}$$

$$\omega = \frac{2}{L}\sqrt{2gD_0} \tag{27}$$

$$A = \frac{L^4 - R_0^4}{L^4 + R_0^4} \tag{28}$$

where R_0 ranges from 0 to L. Thus, A varies between 0 to 1.

Using these, the exact solutions of nonlinear shallow-water equations on polar coordinates (r, θ) are given for flow velocity u and free surface displacement η as:

$$u_\theta = 0 \tag{29}$$

$$u_r = \frac{\omega r\, A\sin\omega t}{2(1-A\cos\omega t)} \tag{30}$$

$$\eta = D_0\left[\frac{(1-A^2)^{1/2}}{1-A\cos\omega t} - 1 - \frac{r^2}{L^2}\left\{\frac{1-A^2}{(1-A\cos\omega t)^2} - 1\right\}\right] \tag{31}$$

The distance R_s from the center of bowl to the coastline is also given as:

$$R_s = L\left[\frac{1-A\cos\omega t}{(1-A^2)^{1/2}}\right]^{1/2} \tag{32}$$

The initial conditions for the numerical simulation are found from (29)~(31) by setting t=0. Various parameters used in the calculation are listed as:

$$D_0 = 1m, \quad L = 2.5km, \quad R_0 = 2km, \quad \Delta x = \Delta y = 25m, \quad \Delta t = 1.25\text{sec} \tag{32}$$

The computational domain of 8km × 8km area is discretized by 320 × 320 uniform grids, and the bottom friction terms in the shallow-water equations are dropped in accordance with the Thacker's analysis. The angular frequency ω and the nondimensional parameter A are found as 3.54×10^{-3} rad/sec and 0.419, respectively. Thus, the period of free oscillation T is 1773sec.

Fig. 6 presents the comparisons of calculated and exact free surface profiles for half period from the initiation of oscillation at each eighth period. The initial convex shape of water surface evolves to a concave surface profile, and the shoreline moves outward as the time increases. A reasonably good agreement is observed between numerical and exact solutions.

Fig. 7 shows the temporal variation of free surface for the second half period of oscillation. The numerical solution deviates slightly from the exact solution due to numerical errors accumulated for one period of oscillation. This errors can be reduced by employing a fine grid system.

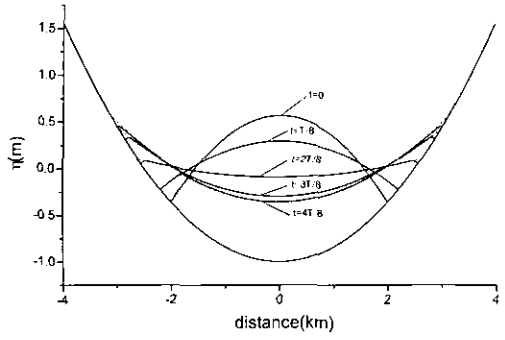

Fig. 6. Comparison of calculated and analytical free surface at t/T= 0, 1/8, 2/8, 3/8, 4/8; ——— calculated, - - - - - - exact (Thacker, 1981).

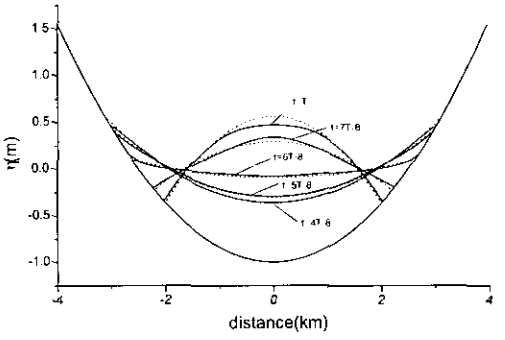

Fig. 7. Comparison of calculated and analytical free surface at t/T= 4/8, 5/8, 6/8, 7/8,1; ——— calculated, - - - - - - exact (Thacker, 1981)

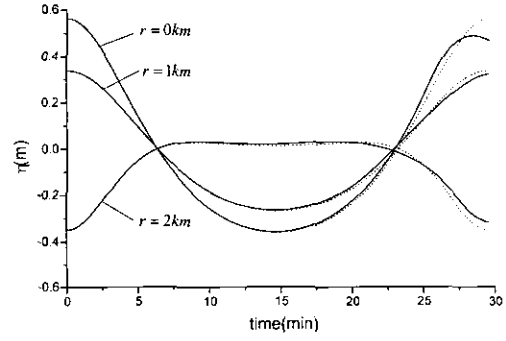

Fig. 8. Time history of free surface displacement at r=0, 1km and 2km; ——— calculated, - - - - - - exact (Thacker, 1981).

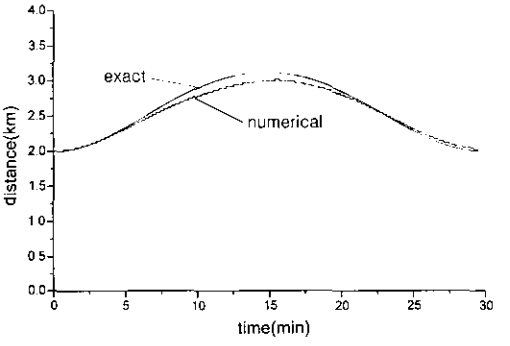

Fig. 9. Time history of coastline change along θ = 0° ; calculated, - - - - - - exact (Thacker, 1981).

Fig. 8 presents the time history of free surface displacements at the center of bowl and the point located 1km apart from the center. Fig. 9 shows the comparison of simulated and analytical shoreline changes with time. Finally, the shape of free surface at each eighth period is visualized for the first half period in Fig. 10.

The comparison of numerical and exact solutions shows that the numerical model is reasonably accurate and can be applied to the simulation of long wave run-up and run-down problems in the coastal area with natural beach.

Fig. 11 presents the three-dimensional plot of free surface profile at the instance when the numerical solution of Imamura(1996) becomes unstable. The instability starts first near moving boundary during the run-down process and it grows with time as shown in Fig 12. This instability is triggered by the discontinuity of nonlinear effect near the boundary in the numerical model of Imamura(1996). The advection terms are evaluated using upwind scheme, and they are very complicated due to the need of additional information on the dry cells when the water flows down the slope. Thus, these terms are dropped for rundown phase of free oscilla-

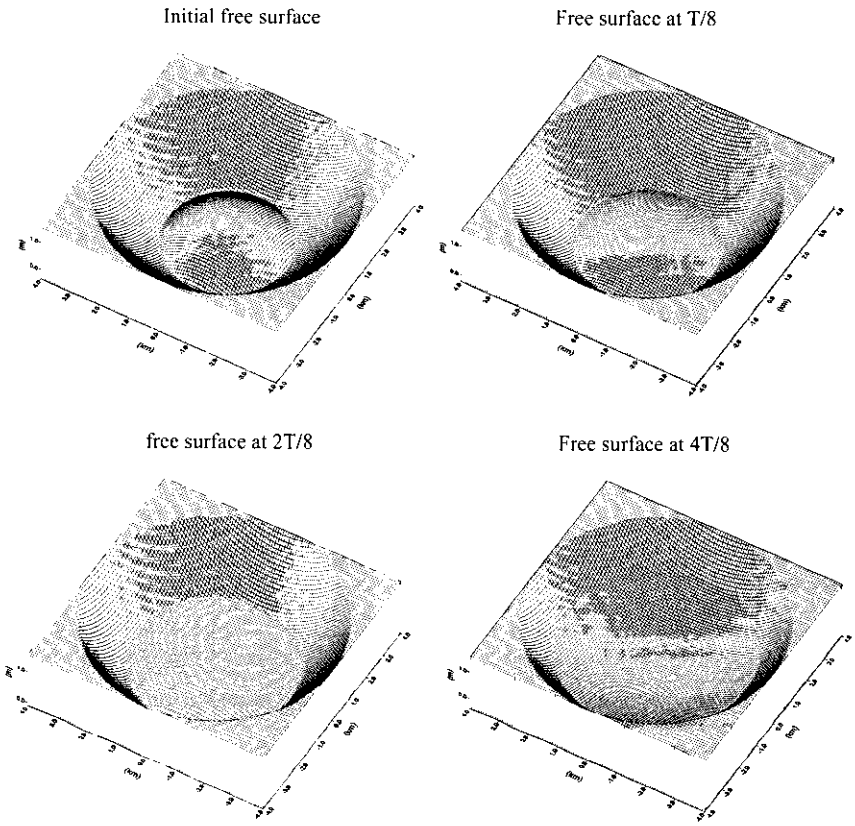

Fig. 10. Instantaneous free surface at t/T=0, 1/8, 2/8 and 4/8

tion for simplicity in his model.

The importance of nonlinear effects across the boundary can be estimated using the analytical solution as:

$$\left| u\frac{\partial u}{\partial r} \right| = \left[\frac{\omega A \sin \omega t}{2(1 - A\cos \omega t)} \right]^2 r \qquad (33)$$

(33) shows that the magnitude of advection term increases linearly with the distance from the center of bowl, and reaches the maximum at the boundary. Thus, the discontinuity of nonlinear effect is inherent when this term is dropped for 3 cells adjacent to the boundary. The numerical model of Tohoku University employing Imamura scheme can still be successfully applied to the inundation simulation in practice, because the bottom friction effect prevents the instability from growing to some extent. However, the de-

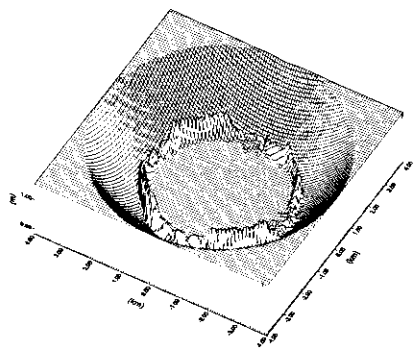

Fig. 11. Instantaneous free surface at 1375sec calculated using Imamura(1996) scheme

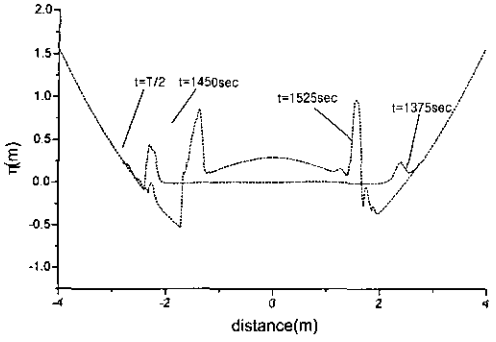

Fig. 12. Free surface calculated using Imamura scheme during run-down process

generation of accuracy is expected.

6. APPLICATION TO DISCONTINUOUS DEPTH REGION

To test the applicability of the present numerical model to the actual inundation problem, a simple conceptual topography is chosen as shown in Fig. 13.

The water depth is described as:

$$h=\begin{cases} 10 & if \quad x \le x_1 \\ 10-20\dfrac{x-x_1}{x_2-x_1} & if \quad x_1 < x \le x_2 \\ -10 & if \quad x > x_2 \end{cases} \tag{34}$$

where,

$$x_1 = 300, \qquad x_2 = 600+150\left[1-\cos\left(\frac{2\pi y}{900}\right)\right] \tag{35}$$

A tidal barrier with top elevation of 4.3m is constructed along x_b = 600m. The barrier has vertical walls on both sides such that the depth is discontinuous along the barrier.

Along the open boundary($x = 0$) the free surface displacements associated with the long waves of 1hr wave period incident normally on

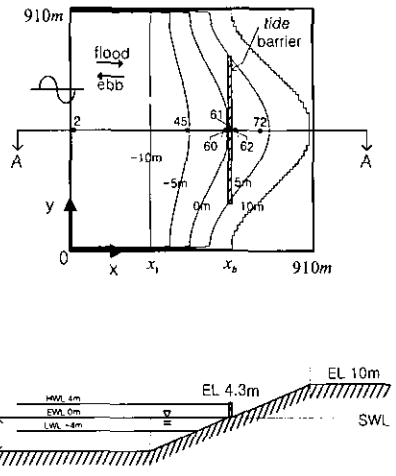

Fig. 13. Simplified topography for simulation of inundation over tidal barrier

the computational area are specified as:

$$\eta(t) = a\cos\left(\frac{2\pi t}{T}\right) \tag{36}$$

$$a=\begin{cases} 4.0 & if \quad 0 < t < 900\,\text{sec} \quad or \quad t \ge 4500\,\text{sec} \\ 4.4 & if \quad 900 < t < 4500\,\text{sec} \end{cases} \tag{37}$$

The amplitude of waves is increased 0.4m for one wave period (i.e., 900 〈 t 〈 4500sec) to generate some overflow on the crest of tidal barrier.

The computational domain of 910m × 910m is discretized by a uniform mesh with 10m grid size. The computation starts with the high tide. Thus, the water surface elevation and the volume fluxes P and Q are initially imposed as:

$$\eta=\begin{cases} 4.0 & if \quad x<x_b \quad and \quad -h<4.0 \\ -h & if \quad x \ge x_b \quad or \quad -h>4.0 \end{cases} \tag{38}$$

$$P = Q = 0 \tag{39}$$

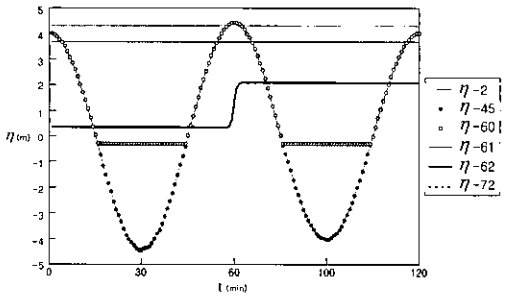

Fig. 14. Time history of water surface at various locations presented in Fig. 13.

Fig. 14 shows the time history of free surface displacements at various locations marked in Fig. 13. The numbers in Fig. 13 denote the grid numbers in the x direction. The grid point No. 2 is located on the open boundary. Thus, the free surface displacement at the point represents the boundary condition imposed for the simulation. Since the point No.45 is submerged and is close to the open boundary, the calculated free surface is almost identical with that of No.2. The point No.61 is located on the crest of tidal barrier whose top elevation is 4.3m. This point is normally exposed, but becomes submerged when the second peak of waves arrives there. The points No.60 and No.62 are the grid points located in the front and rear sides, respectively, of the barrier. The free surface at the point No.60 falls down until the bottom(EL. -0.3m) is touched and remains exposed, for the time being. This point is again submerged when the second wave arrives there. The bottom elevation of point No.62 is -0.3m which is lower than the ordinary high water level(EL. 4m). However, this point is initially exposed, because the tidal barrier protects this area. When second peak of waves arrives and the water flows over the crest of barrier, this area is flooded. After the inundation process is over, a water pool is formed there. The point No.72 is located high above the maximum inundation height, this area is always exposed.

Figs. 15~18 present the velocity vector at various stages of inundation process. For the first ebb motion(Fig. 15), the free surface falls down and the water flows towards the open sea. In the shallow region near the coast line, the velocity vector is more or less concentrated towards the deeper area of the bay. When the low water level is reached as shown in Fig. 16, a large portion of area is exposed, and the flow becomes very weak except for the shallow region where the thin film of water is still in mo-

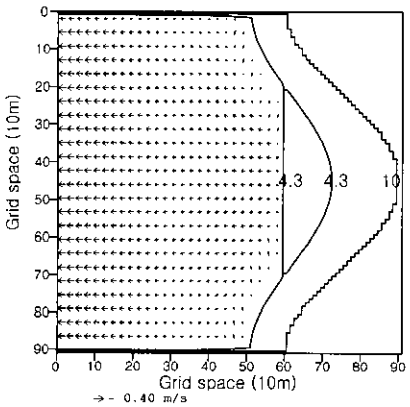

Fig. 15. Velocity vector plot at ebb phase.

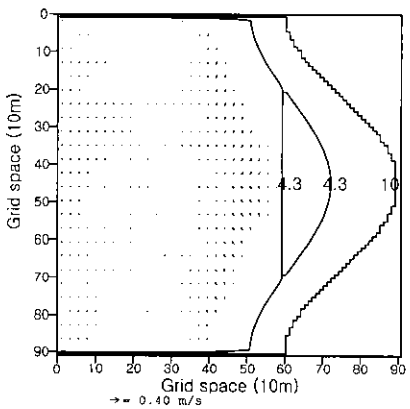

Fig. 16. Velocity vector plot at low water.

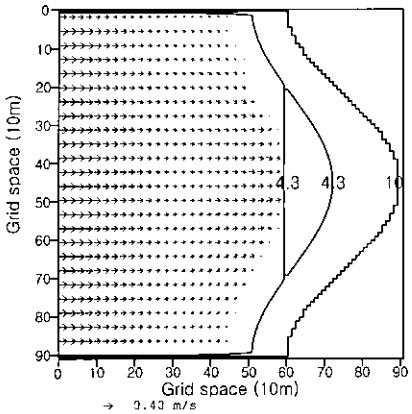

Fig. 17. Velocity vector plot at flood phase.

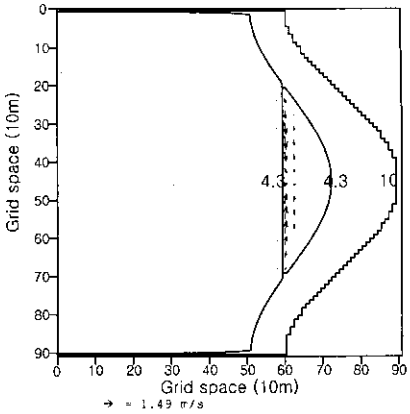

Fig. 18. Velocity vector distribution showing overflow at high tide due to superposition of surge

tion due to high bottom friction.

Fig. 17 shows the velocity distribution for flooding stage due to the surge superposed on the initial ordinary long waves. As shown in Fig. 18, the free surface is higher than the crest of tidal barrier, and the water flows over the barrier. The overtopped water flows down towards the deeper area, and forms finally a water pool there.

Judging from the result presented above, the inundation process over the coastal area with abrupt change of bottom topography can be well described by the numerical simulation. However, a quantative verification of the numerical model is essential prior to the application of present model to actual inundation.

7. CONCUSIONS

The moving boundary technique developed by Imamura(1996) is improved by continuing the nonlinear effects across the boundary between wet and dry cells during run-down process of long waves. The accuracy of present numerical model is tested using the analytical solution of nonlinear shallow water equation for the case of free oscillation inside the parabolic bowl. A good agreement between calculated and analytical results is observed. It is also shown that the instability generated near the boundary grows and ruins eventually the whole computation when the original Imamura scheme is used for the case of no bottom friction. The present numerical model is employed to simulate the coastal inundation over a tidal barrier constructed on a slowly varying topography. The water body motion due to inundation process is well described by the numerical simulation. However, a further research should be done for the complete verification of the present model.

ACKNOWLEDGEMENTS

This research is funded by Korea Science and Engineering Foundation (Grant No. 1999-2-311-005-3).

REFERENCES

Cho, Y.-S.(1995). *Numerical Simulations of Tsunami Propagation and Run-up*, Ph.D. Thesis, School of Civil and Env. Engrg., Cornell University, Ithaca, N.Y.

Goto, C. and Shuto, N.(1983). "Numerical simulation of tsunami propagations and run-up," *Tsunami-Their Science and Engineering*, edited by Iida and Iwasaki, Terra

Science Publishing Company, Tokyo, pp. 439-451.

Imamura, F.(1996). "Review of tsunami simulation with a finite difference method," *Long-wave runup mathematical models*, eds Yeh, Liu & Synolakis, World Scientific, pp. 25-42.

Iwasaki, T. and Mano, A.(1979). "Two-dimensional numerical computation of tsunami run-ups in the Eulerian description," *Proc. of 26th Conf. on Coastal Eng.*, JSCE, pp. 70-74(in Japanese).

Liu, P.L-F., Cho, Y.-S., Yoon, S.B., and Seo, S.N.(1995). "Numerical simulations of the 1960 Chilean tsunami propagation and inundation at Hilo, Hawaii," *Tsunami: Progress in Prediction, Disaster Prevention and Warning*, edited by Tsuchiya and Shuto, Kluwer Academic Publishers, pp. 99-115.

Thacker, W.C.(1981). "Some Exact Solutions to the Nonlinear Shallow Water Wave Equation," *J. of Fluid Mechanics*, vol. 107, pp. 499-508.

Yoon, T.H., Yoon, S.B., Lee, H.J., and Shin, W.T.(1994). "Prediction of flow velocity due to tidal closing," *Proc. of 36th Conf. for Korean Association of Hydrological Sciences*, Yeosu, Korea, pp. 133-138(in Korean).

Sung Bum Yoon, Department of Civil and Environmental Engineering, Hanyang University, Ansan, Kyunggi-Do, 425-791, Korea. (E-mail:sbyoon@email.hanyang.ac.kr)

Ji Hoon Cho, Water Resources and Environmental Research Division, Korea Institute of Construction Technology, 2311 Taehwa-dong, Ilsan-Gu, Goyang, Kyunggi 411-807, Korea

(Received June 27, 2000; accepted March 3, 2001)